



Sedimentology and Geochemistry of the Lower Permian Shanxi Formation Shan 2³ Submember Transitional Shale, Eastern Ordos Basin, North China

Yifan Gu^{1,2}, Xingtao Li³, Lin Qi⁴, Shuxin Li³, Yuqiang Jiang^{1,2*}, Yonghong Fu^{1,2} and Xiaoshuai Yang¹

¹School of Geoscience and Technology, Southwest Petroleum University, Chengdu, China, ²The Unconventional Reservoir Evaluation Department, PetroChina Key Laboratory of Unconventional Oil and Gas Resources, Chengdu, China, ³PetroChina Coalbed Methane Company, Beijing, China, ⁴Geology Exploration and Development Research Institute, CNPC Chuanqing Drilling Engineering Co., Ltd., Chengdu, China

OPEN ACCESS

Edited by:

Shu Jiang,
The University of Utah, United States

Reviewed by:

Caitang Wu,
China University of Mining and
Technology, China
Quanzhong Guan,
Chengdu University of Technology,
China
Ping Hongwei,
China University of Geosciences
Wuhan, China

*Correspondence:

Yuqiang Jiang
xnsyjyq3055@126.com

Specialty section:

This article was submitted to
Economic Geology,
a section of the journal
Frontiers in Earth Science

Received: 21 January 2022

Accepted: 07 February 2022

Published: 25 February 2022

Citation:

Gu Y, Li X, Qi L, Li S, Jiang Y, Fu Y and
Yang X (2022) Sedimentology and
Geochemistry of the Lower Permian
Shanxi Formation Shan 2³
Submember Transitional Shale,
Eastern Ordos Basin, North China.
Front. Earth Sci. 10:859845.
doi: 10.3389/feart.2022.859845

Shanxi Formation Shan 2³ Submember transitional shale in Eastern Ordos Basin is characterized by high TOC value, wide distribution, and large single-layer/cumulative thickness. In this study, based on section division of Shan 2³ Submember, petrographic, mineralogical, and high-resolution geochemical analyses were integrated to reveal sedimentary environment, detrital influx, paleoclimate, paleosalinity, and paleoredox conditions. Results indicate that Shan 2³ Submember is divided into four sections (Shan 2³-1, Shan 2³-2, Shan 2³-3, and Shan 2³-4). The upper part of the Shan 2³-1 section is dominated by bay facies, which is characterized by high TOC value (2.75%–10.96%, avg. 6.98%), low detrital influx proxies (Zr, 97–527 ppm, avg. 310 ppm; Ti, 1985–7591 ppm, avg. 3938 ppm), relatively dry paleoclimate condition (CIA*, 41.96–92.58, avg. 75.55; Sr/Cu, 6.23–14.49, avg. 8.87), high paleosalinity proxies (Sr/Ba, 0.39–1.29, avg. 0.62), and relatively anoxic reduction condition (U_{EF}, 0.83–3.00, avg. 1.67; Mo_{EF}, 3.95–27.00, avg. 15.56). By comparison, the other three sections are dominated by a combination of transitional facies, including barrier island, lagoon, tidal flat, and swamp. In this interval, shale is deposited in lagoon facies. The paleoclimate gradually tends to be warm and humid, which results in increasing the chemical weathering intensity. Meanwhile, the detrital influx increases, and the paleoredox condition tends to be oxic. The above conditions are not conducive to the preservation of organic matter in lagoon facies shale.

Keywords: Permian, transitional facies, geochemistry, organic-rich shale, Ordos basin, Shan 2³ Submember

INTRODUCTION

As an indispensable part of petroliferous basins, organic-rich shales play the role of source rocks and unconventional oil and gas reservoirs (Berry, 2010; Qiu et al., 2016; Sun et al., 2017; Guan et al., 2019; Zou et al., 2019; Zhang et al., 2020; Tang et al., 2021). Previous studies suggested that organic-rich shales can be formed in marine, continental, and marine-continental transitional environments, including bays, lagoons, deep shelves, semi-deep lakes, and deep lakes (Zou et al., 2015; Yang et al., 2017; Luo et al.,

2018; Zhang et al., 2018; Wei et al., 2021). At present, marine shales are dominant in the known shale oil and gas reservoirs and have achieved large-scale and efficient development in the United States, Canada, and China (Zou et al., 2015; Qiu and Zou, 2020; Guan et al., 2021). However, there are relatively few reports of marine-continental transitional shale (Liang et al., 2018), which are limited to the Mesozoic and Cenozoic shales in the Powder River, the Gulf of Mexico, Sacramento and San Juan basins in the United States (Dong et al., 2021), the Bonaparte Basin in Australia (Hou et al., 2015), and Southern North China Basin and the Ordos Basin in China (Li et al., 2017; Liang et al., 2018; Li et al., 2019; Kuang et al., 2020).

The Permian marine-continental transitional shale of the Shanxi Formation in the Ordos Basin has the characteristics of large single-layer thickness, high organic matter abundance, moderate maturity, and good gas content (Kuang et al., 2020). It has huge geological resources and is expected to become a new strategic alternative resource for China's natural gas industry. The Shanxi Formation Shan 2³ Submember transitional facies shale is characterized by high TOC value, wide distribution, and large single-layer/cumulative thickness, which is the key target for the exploration and development of shale gas in the Ordos Basin (Kuang et al., 2020; Zhang et al., 2021). At present, the geological study on the transitional shale of the Shanxi Formation is still in the early stage (Dong et al., 2021). Previous studies concentrated on the evaluation of different lithofacies (Wu et al., 2021), macroscopic reservoir characteristics (Wei et al., 2020), microscopic pore structure, and gas content (Sun et al., 2017). Meanwhile, a few studies have been carried out on the sedimentary model of transitional shale, and many viewpoints have been proposed, including the lagoon model (Dong et al., 2021; Zhang et al., 2021), tide-dominated delta front model (Kuang et al., 2020), and bay model (Wu et al., 2021). However, due to the various types of sedimentary facies in the transitional environment, the rapid spatial variation, and the lack of systematic studies on unconventional oil and gas sedimentology, the corresponding geochemical study is rare. The development characteristics and distribution of organic-rich shale in transitional facies are unclear, and the sedimentary model of organic-rich shale is still controversial.

Geochemical analysis has been widely applied to reveal the paleoredox condition, paleosalinity, paleo-water depth, paleoproductivity, and detrital influx effect of organic-rich shales (Chen et al., 2020; Zhang et al., 2020; Zhang et al., 2021). Based on the section division of the Shan 2³ Submember, this study combined high-resolution geochemical analyses with sedimentary facies characteristics (including petrology, mineral composition, TOC, major and trace elements, and key proxies) to discuss sedimentary environment (including detrital influx, paleosalinity, paleoredox, and paleoclimate condition) of the transitional shale in each section of the Shan 2³ Submember. This study has reference and guiding significance for the exploration and development of transitional shale gas.

GEOLOGICAL SETTING

The Ordos Basin, with an area of 370,000 km², is a typical cratonic basin developed on the Archean granulites and Lower

Proterozoic greenschists of the North China Craton (Zhang et al., 2021) (**Figure 1A**). The Ordos Basin can be divided into six secondary structural units: Yimeng Uplift, Western Fold-Thrust Belt, Tianhuan Depression, Shenbei Slope, Jinxi Flexural Fold Belt, and Weibei Uplift.

The study area, with an area of 4.5×10^4 km², is located in the Eastern Ordos Basin (**Figure 1B**). During the Late Carboniferous period, the North China Craton continued to subside, while the North China sea transgressed into the eastern part of the basin in the N-S direction, creating a littoral shallow marine depositional environment. During the Early Permian Taiyuan Formation period, the transgression expanded and overlaid the central paleo-uplift to produce a unified epicontinental sea (Wu et al., 2021). During the Early Permian Shanxi Formation period, influenced by the Hercynian tectonic movement, the North China Craton uplifted as a whole, and the seawater gradually exited from the basin from both sides of the east and west. It was a transitional sedimentary stage between marine and continent under the background of the epeiric platform (Wu et al., 2021). Affected by tidal activities, the sedimentary system of the shore-shallow sea, lagoon, and tide-controlled delta was developed. To the Middle Permian Xiashihezi Formation period, the study area entered the continental sedimentary evolution stage with complete regression (Chen H et al., 2011). The Lower Permian Shanxi Formation is divided into the Shan 1 Member and Shan 2 Member. The Shan 2 Member is further divided into Shan 2¹ Submember, Shan 2² Submember, and Shan 2³ Submember. The Shan 2³ Submember is mainly composed of black and gray-black organic-rich shale, which is the target interval for shale gas exploration in the Eastern Ordos Basin. The Shan 2³ Submember is further divided into four sections: Shan 2³-1, Shan 2³-2, Shan 2³-3, and Shan 2³-4 (**Figure 1C**).

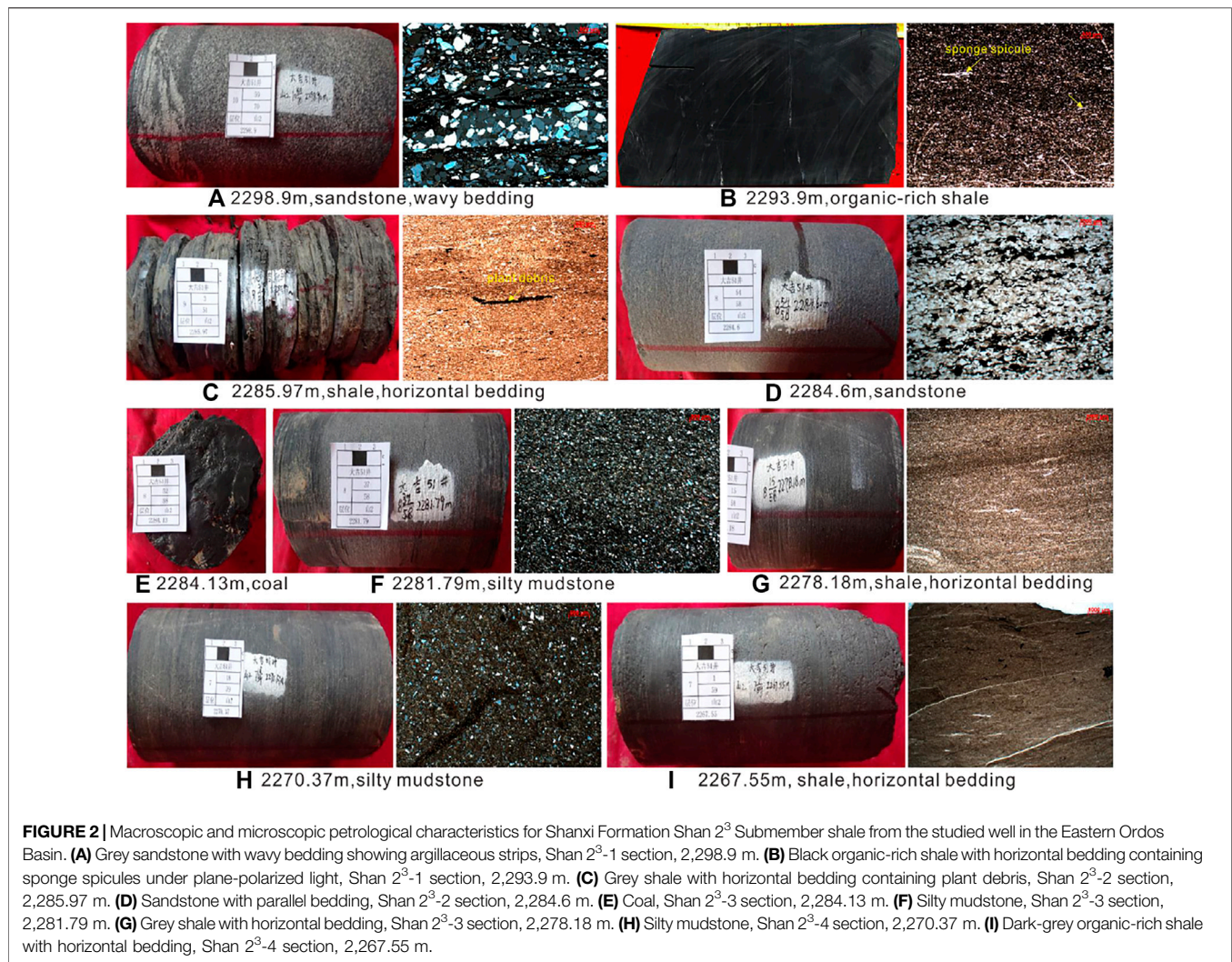
METHODS

Sedimentological Characterization

The studied well carried out continuous coring in Shan 2³ Submember. Core observation identified a different lithology, including coal, fine-grained sandstone, siltstone, silty mudstone, shale, and recorded the lithology combination of different sections. One hundred twenty-five thin sections of core samples were made, and the core observation results were further verified by Leica DM4 M optical microscope. Observation and description of typical sections were made in the study area, emphasizing sedimentary texture or structure.

Organic Matter Contents Analysis

TOC was measured by Leco carbon/sulfur analyzer in PetroChina Key Laboratory of Unconventional Oil and Gas Resources, and the analytical precisions are $\pm 0.5\%$. The samples were treated with 10% hydrochloric acid to remove carbonates. The acid-treated sample was washed with distilled water to neutralize. Then, the sample was dried in an oven at 60°C–80°C. Dried samples were added to the cosolvent and fully burned in the high-temperature oxygen flow, ensuring that the organic carbon could be completely converted into carbon dioxide, and the content of total organic carbon was tested by an infrared detector.



(GSD-9) was used to monitor the analytical accuracy and precision.

Authigenic enrichment of the redox-sensitive trace elements was widely used to indicate redox changes in the water column (Algeo and Tribouillard, 2009; Algeo and Liu, 2020). The enrichment factor (EF) is calculated by comparing the Al-normalized metal concentration to those of the continental crust (Wedepohl, 1995). The calculation formula is as follows:

$$X_{EF} = (X/Al)_{\text{sample}} / (X/Al)_{CC} \quad (2)$$

X represents the concentration of element X , and $(X/Al)_{CC}$ represents the X/Al ratio of the continental crust (Wedepohl, 1995).

RESULTS

Sedimentological Characteristics

Shan 2³-1 Section

The lower part of the Shan 2³-1 section of the studied well comprises frequent interbeds of grey silty mudstone and

sandstone characterized by wavy bedding (Figure 2A). There are argillaceous bands between siltstones, representing the tidal flat environment with frequent changes in energy. The above characteristics are also observed in Chengjiazhuang Outcrop and Taitou Outcrop (Figures 3A,B). The upper part of the Shan 2³-1 section comprises the grey-black organic-rich shale (Figure 2B), and the bedding structure is not developed. Marine bioclastics, such as ostracods, brachiopods, and crinoids, can be identified in hand specimens (Figure 3C), reflecting the marine bay environment (Figure 4).

Shan 2³-2 Section

The observation results on the studied well and outcrops show that the lower part of the Shan 2³-2 section comprises dark grey shale with horizontal bedding (Figure 2C). Many plant debris can be seen inside, representing the lagoon facies (Figure 2C). The upper part of this section comprises grey fine-grained sandstone and develops massive bedding (Figure 2D), representing barrier islands. Nevertheless, the

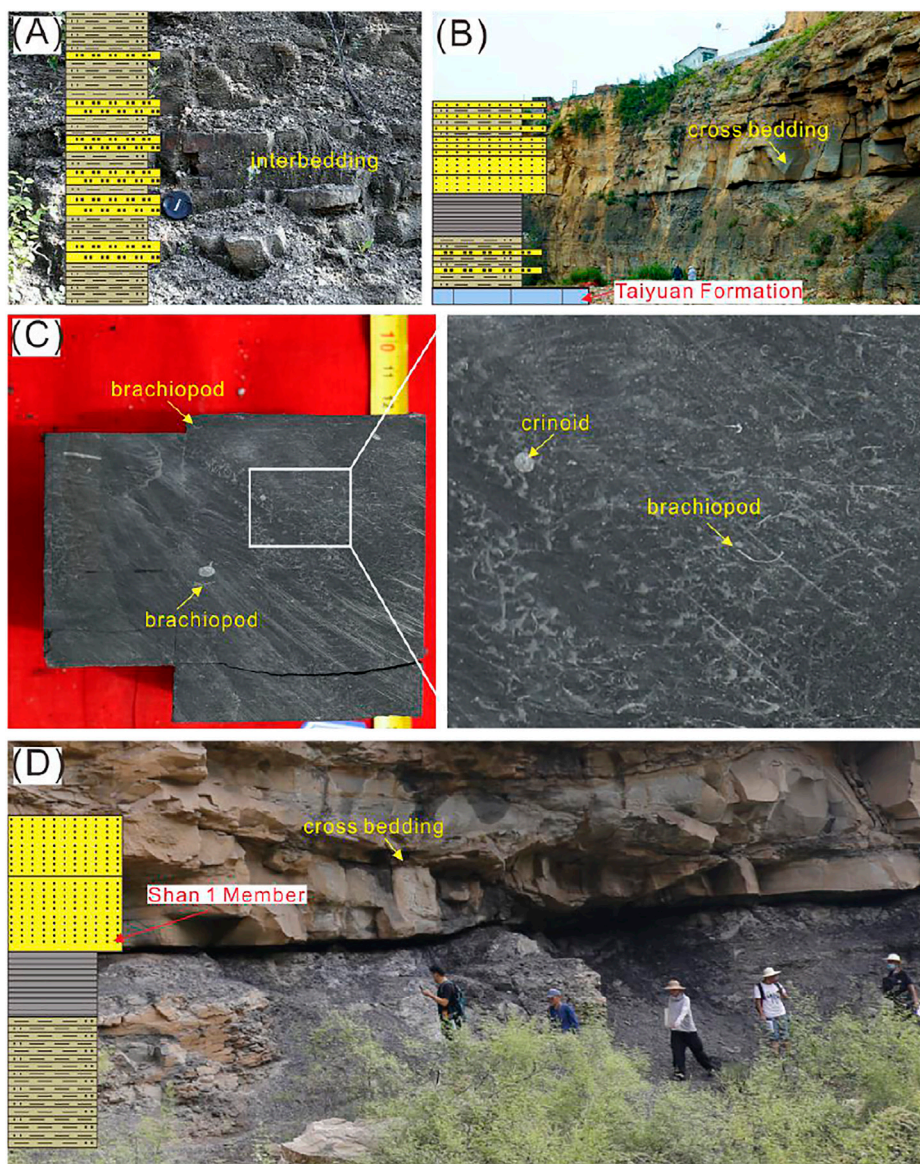


FIGURE 3 | Sedimentary characteristics for Shanxi Formation Shan 2³ Submember shale from outcrops in the Eastern Ordos Basin. **(A)** Frequent thin interbeds of siltstone and silty mudstone, Shan 2³-1 section, Taitou Outcrop. **(B)** Medium-grained sandstone with cross-bedding, Shan 2³-1 and Shan 2³-2 sections, Chengjiazhuang Outcrop. **(C)** Organic-rich shale containing abundant marine bioclasts including crinoid and brachiopod, Shan 2³-1 section, 2,294.89 m, studied well. **(D)** Shan 2³-4 section, Chengjiazhuang Outcrop.

upper part of the Shan 2³-2 section in Chengjiazhuang Outcrop is dark yellow thick medium-coarse grained sandstone with large cross-bedding (**Figure 3B**). The scour surface of the medium-coarse grained sandstone can be observed at the bottom, and the top is flat (**Figure 3B**), reflecting the delta front environment (**Figure 4**).

Shan 2³-3 Section

The lithologic column of the Shan 2³-3 section in the studied well consists of a vertical variation of black coal (**Figure 2E**), grey silty mudstone, and dark grey shale. Coal represents a swamp, while silty mudstone represents a tidal flat (**Figure 2F**).

Shale with horizontal bedding represents a lagoon (**Figure 2G**). Vertical lithology changes reflect rapid changes of the transitional environment under sea level changes (**Figure 4**).

Shan 2³-4 Section

The lithology column of the Shan 2³-4 section in the studied well also shows the vertical rapid change between black coal, grey silty mudstone (**Figure 2H**), and dark grey shale (**Figure 2I**). Coal interval represents a swamp, silty mudstone represents a tidal flat, and shale with horizontal bedding represents lagoon facies (**Figure 3D**).

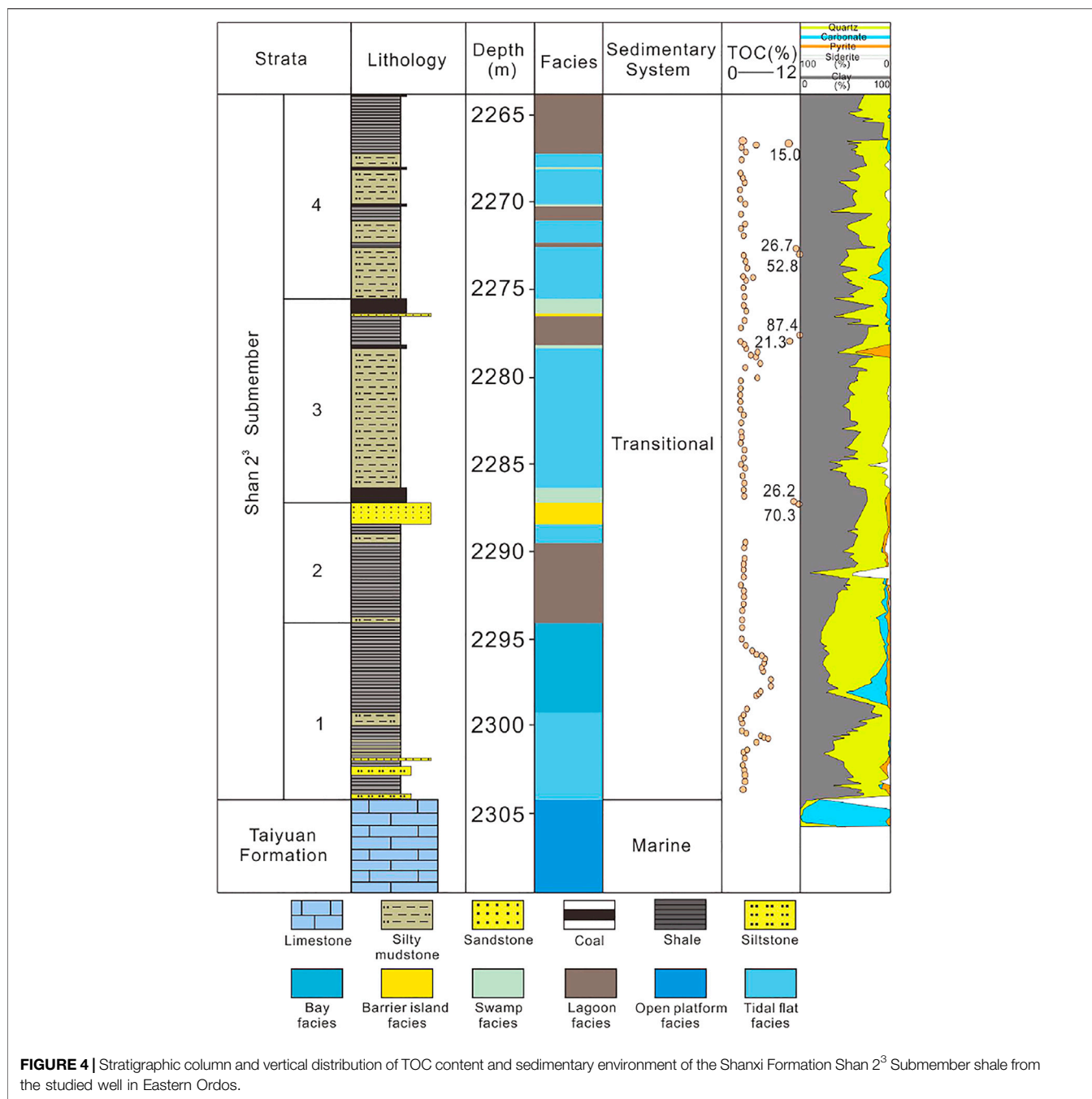


FIGURE 4 | Stratigraphic column and vertical distribution of TOC content and sedimentary environment of the Shanxi Formation Shan 2³ Submember shale from the studied well in Eastern Ordos.

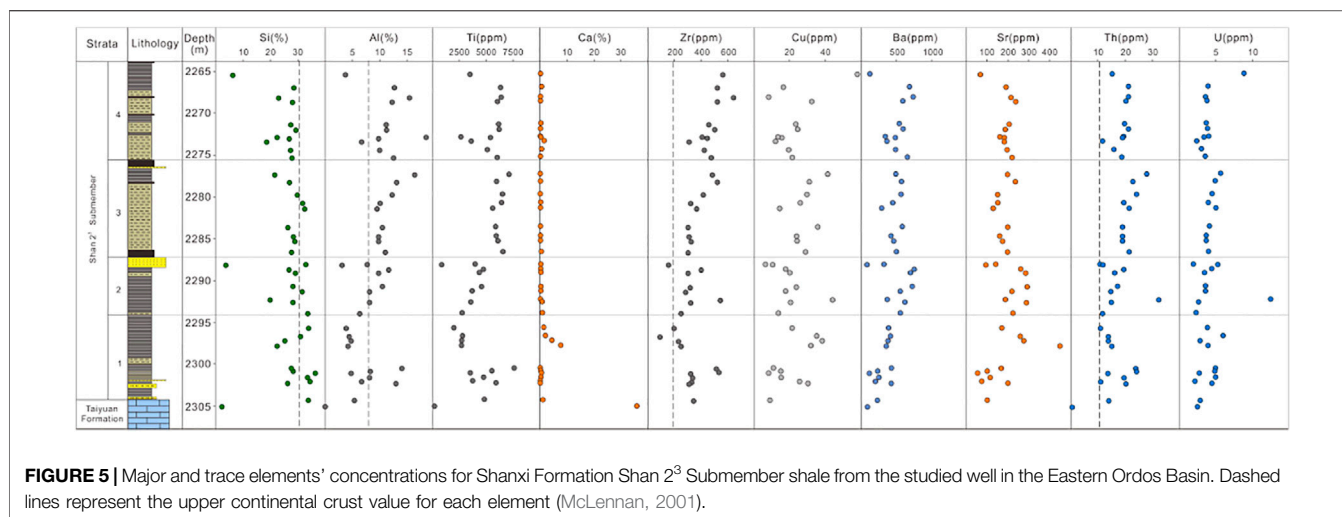
TOC Content Characteristics

Based on testing results of transitional shale and coal, this study sorted out the TOC changes in each section of the Shan 2³ Submember (Figure 4). There is no coal interval in the Shan 2³-1 section, and the TOC of transitional shale varies widely, ranging from 0.26% to 10.96%, with an average of 5.11% (n = 12). The high TOC values are concentrated in 2,292.35–2,298.27 m. The B layer also does not develop coal seam. The TOC range of transitional shale in the Shan 2³-2 section is small, distributed in 0.59%–2.14%; the average is only 1.41% (n = 6). In the Shan 2³-3 section, the TOC value of coal interval is up to 21.26%.

However, the range of the transitional shale is only 0.14%–7.32%, with an average of 1.83% (n = 9). In the Shan 2³-4 section, the TOC value of the coal interval is up to 15.03%, and the range of transitional shale is only 0.24%–2.55%, with an average of 1.57% (n = 11).

Major Element Geochemistry

The variation trend of the major element concentration in different sections of the Shan 2³ Submember is obvious (Figure 5). The Ca concentration of the Shan 2³-1 section is higher than that of other sections. The Ca concentration ranges



from 0.10% to 7.64%, with an average of 1.62% ($n = 11$). The Ca concentration in the Shan 2³-2 section is 0.16%–0.85%, with an average of 0.43% ($n = 9$). The average Ca concentration in a high TOC interval (2,292.35–2,298.27 m) is 2.06%. The Ca concentration in the Shan 2³-3 section is 0.09%–0.54%, with an average of 0.22% ($n = 10$). The Ca concentration in the Shan 2³-4 section is 0.11%–1.57%, with an average of 0.41% ($n = 11$).

The Al concentration of the Shan 2³-1 section is the lowest, but the Si concentration is the highest (Figure 5). The average Al concentration and Si is 7.25% (4.17%–14.08%, $n = 11$) and 30.58% (22.61%–36.87%, $n = 11$), respectively. The average concentration of Al and Si in the Shan 2³-2 section is 9.57% (3.42%–19.29%, $n = 9$) and 26.41% (3.63%–33.98%, $n = 9$), respectively. The average concentration of Al and Si in the Shan 2³-3 section is 11.63% (9.69%–16.34%, $n = 10$) and 28.31% (21.71%–32.90%, $n = 10$), respectively. The average concentration of Al and Si in the Shan 2³-4 section is 11.38% (4.01%–18.39%, $n = 11$) and 24.37% (6.18%–29.64%, $n = 11$), respectively. The average concentration of Ti and Zr in the Shan 2³-1 section is 4178 ppm (1985–7591 ppm, $n = 11$) and 315 ppm (97–527 ppm, $n = 11$), respectively. The average concentration of Ti and Zr in the Shan 2³-2 section is 4185 ppm (840–9309 ppm, $n = 9$) and 460 ppm (159–1558 ppm, $n = 9$), respectively. The average concentration of Ti and Zr in the Shan 2³-3 section is 6198 ppm (5592–7120 ppm, $n = 10$) and 386 ppm (305–520 ppm, $n = 10$), respectively. The average concentration of Ti and Zr in the Shan 2³-4 section is 5205 ppm (2,611–6,378 ppm, $n = 11$) and 478 ppm (313–636 ppm, $n = 11$), respectively.

Trace Element Geochemistry

The concentration of indicator trace elements or their ratios have been widely used to analyze the paleoredox conditions, paleosalinity, paleoclimate, and paleoproductivity of sedimentary environment. The changes of trace elements and sedimentary environment geochemical indicators of transitional shale in each section are shown in Figures 5, 6. The CIA of the Shan 2³-1 section is the lowest, ranging from 41.96 to 91.58, with an average of only 78.92 ($n = 11$). The CIA values of the Shan 2³-

2, Shan 2³-3, and Shan 2³-4 sections are similar, and the average values are 85.00 (78.58–94.79, $n = 9$), 87.10 (83.76–92.53, $n = 10$), and 85.63 (75.68–95.63, $n = 11$), respectively. The change trend of Sr/Cu is similar to that of CIA. The Sr/Cu of the Shan 2³-1 section is relatively low, ranging from 2.91 to 14.49, and the average value is only 8.28 ($n = 11$). The average Sr/Cu ratios in the Shan 2³-2, Shan 2³-3, and Shan 2³-4 sections are 12.75 (4.28–19.91, $n = 9$), 6.54 (4.81–8.62, $n = 10$), and 10.68 (1.19–24.18, $n = 11$), respectively.

The variation trends of Sr/Ba, U_{EF} , Mo_{EF} , and U/Th are opposite to those of CIA* and Sr/Cu (Figure 6). The average values of Sr/Ba, U_{EF} , and Mo_{EF} in the Shan 2³-1 section are 0.57 (0.39–1.29, $n = 11$), 14.63 (7.12–30.07, $n = 11$), and 126.18 (39.53–270.27, $n = 11$), respectively, which are significantly higher than those of the other three sections. The average values of U/Th in each section are similar, and the average values of the Shan 2³-1, Shan 2³-2, Shan 2³-3, and Shan 2³-4 sections are 0.24 (0.19–0.43, $n = 11$), 0.25 (0.17–0.44, $n = 9$), 0.20 (0.18–0.23, $n = 9$), and 0.22 (0.17–0.58, $n = 11$), respectively.

DISCUSSION

Detrital Influx Proxies

As an important element in rocks, the concentrations of Al, Ti, and Zr in rocks are almost not affected by weathering or diagenesis, so they are used to evaluate the impact of detrital influx (Li et al., 2017; Liu et al., 2021; Zhang et al., 2021). Al only exists in the clay minerals of fine-grained sedimentary rocks, while Ti and Zr are mainly assigned to clay, sand, and silt particles composed of ilmenite, rutile, and augite (Caplan and Bustin, 1998; Murphy et al., 2000). The detrital influx proxies, including Al, Ti, and Zr, are generally low in the Shan 2³-1 section (Figure 5), especially in the high TOC interval (2,292.35–2,298.27 m). It is suggested that the terrestrial input in the Shan 2³-1 section has little effect, which benefits the enrichment of marine fauna and corresponding organic matter. However, unlike other proxies, the Si concentration is high in the Shan 2³-1 section (Figure 5), suggesting that biogenic silicon

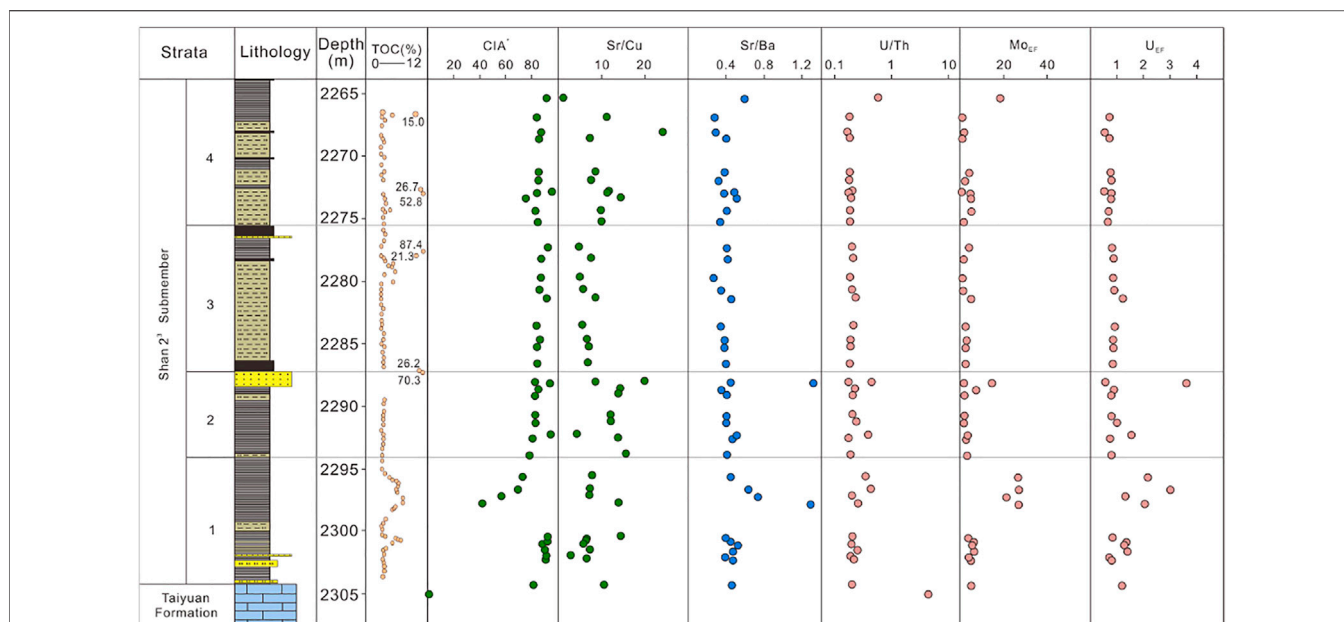


FIGURE 6 | TOC and trace elements ratios for Shanxi Formation Shan 2³ Submember shale from the studied well in the Eastern Ordos Basin.

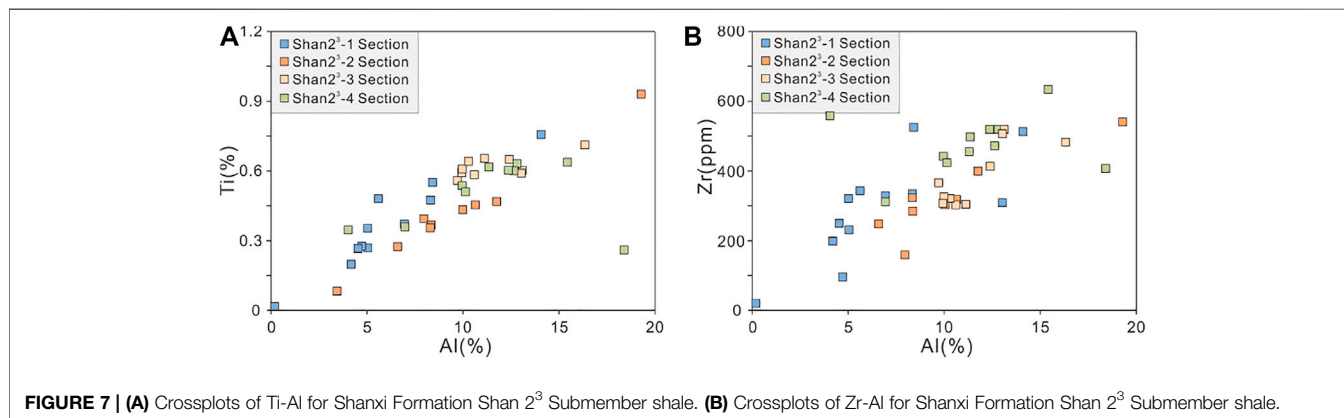


FIGURE 7 | **(A)** Crossplots of Ti-Al for Shanxi Formation Shan 2³ Submember shale. **(B)** Crossplots of Zr-Al for Shanxi Formation Shan 2³ Submember shale.

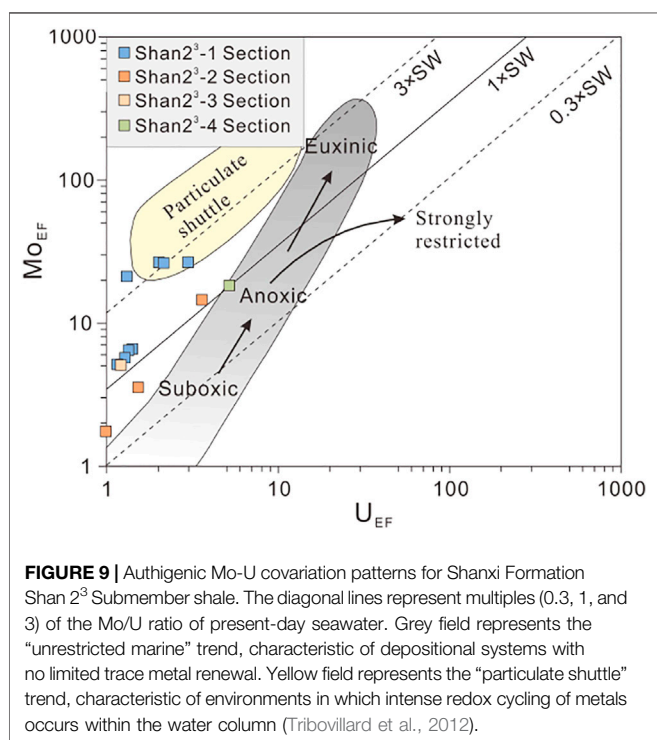
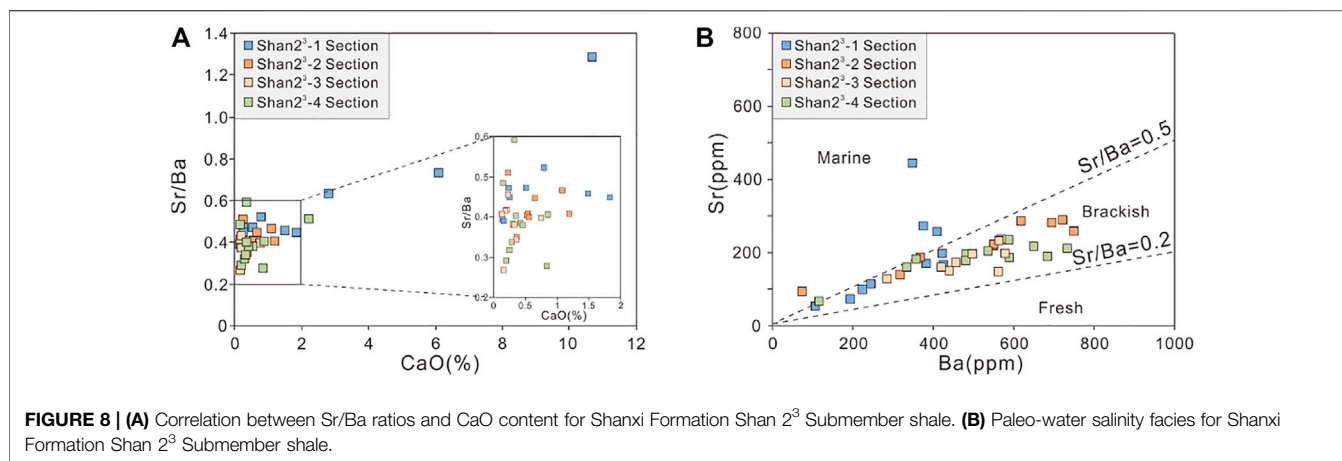
accounts for a considerable part. In contrast, the other three sections are greatly affected by detrital influx (**Figure 5**), which enters the deposition process of transitional shale through deltas and tidal channels. Zr/Al and Ti/Al ratios are thought to closely relate to the coarser part of the sediments (Bertrand et al., 1996; Caplan and Bustin, 1998). Good Ti-Al correlation indicates that Ti comes from the lattice of clay minerals or stable terrigenous clastic materials (Zhang et al., 2021). Zr usually exists in clay minerals or heavy minerals of silt size (e.g., zircons) (Rachold and Brumsack, 2001; Liu et al., 2017). Al and Ti show a good correlation in each section (**Figure 7A**), but the correlation between Al and Zr is poor in each section (**Figure 7B**).

Paleoclimate Conditions

Paleoclimate not only affects ocean currents, water stratification, parent rock weathering, sediment erosion, and

transport but also has an important impact on the species and population density of marine fauna (Zhang et al., 2005). The warm-humid climate is conducive to the atmospheric water cycle, accelerating the chemical weathering intensity, and causing the transportation of nutrients to marine or lake. In addition, a warm-humid climate is conducive to the prosperity of microorganisms in surface water and the burial amount of organic matter (Chen D et al., 2011).

Because the paleoclimate changes will affect the chemical composition of rocks to some extent, the paleoclimate of the sedimentary period can be reflected by the change of chemical composition of rocks in turn. Sr and Cu are very sensitive to climate, so the contents of these two elements can be used to reflect the paleoclimate conditions of sediments. Sr is likely to be lost due to weathering and leaching, while Cu is relatively stable (Zhang et al., 2021). Under warm conditions, due to strong



chemical weathering, Sr is more easily lost, resulting in increased Sr/Cu in sediments. Under dry and hot conditions, the weathering intensity is relatively low, and more Sr elements remain in the parent rock, resulting in lower Sr/Cu values in sediments. The Sr/Cu ratio can be used to evaluate paleoclimatic conditions. For a dry and hot climate, the Sr/Cu ratio is between 1 and 5, while for a warm and humid climate, the Sr/Cu ratio is greater than 5 (Sarki Yandoka et al., 2015; Xu et al., 2017; Xie et al., 2018). The average Sr/Cu ratio of the Shan 2³-1 section is only 8.28; especially, the Sr/Cu ratio of high TOC interval is the lowest in Shan 2³ Submember (Figure 6). It is suggested that a relatively dry climate leads to a less detrital influx, which is conducive to the formation of organic-rich shale. The Sr/Cu ratio of the Shan 2³-2 section is significantly higher than that of

the Shan 2³-1 section, indicating that the climate tends to be warm and humid (Figure 6).

CIA has been widely used to evaluate the chemical weathering intensity (Nesbitt and Young, 1982; Bai et al., 2015). In general, high CIA values suggested warm, humid paleoclimate and strong chemical weathering. Low CIA values reflect dry and cold paleoclimate and weak chemical weathering. Bai et al. (2015) proposed that when CIA was 50–65, it reflected the dry-cold climate under the background of low chemical weathering. When CIA is 65–85, it reflects the warm-wet climate under the background of moderate chemical weathering. When CIA is 85–100, it reflects the hot and humid paleoclimate under strong chemical weathering. The CIA* of the Shan 2³-1 section is the lowest (Figure 6), which is in the middle range of chemical weathering, indicating that when the Shan 2³-1 section is deposited, the climate is relatively dry, which is not conducive to chemical weathering. The CIA* values of the other three sections are similar (>85), which indicate that the climate tends to be warm and humid. It is conducive to improving the chemical weathering intensity. This scenario is also proved by the variation trend of the Sr/Cu ratio (Figure 6).

Paleo-Water Salinity

Paleosalinity records the salinity of ancient water in the sedimentary period, which provides important information for analyzing the sedimentary environment. Sr and Ba were considered two indicator elements sensitive to paleosalinity (Wang et al., 1979; Wang, 1996). Sr and Ba showed different enrichment in different sedimentary environments. In low salinity water, Sr and Ba existed in the soluble bicarbonate. With the increase of salinity, Ba gradually precipitated in the form of BaSO₄, and the Ba concentration in water decreased compared with Sr (Wolgemuth and Broecker, 1970). In higher salinity waters, Sr is precipitated only in the form of SrSO₄ (Wang et al., 1979). The enrichment of Sr in sediments is associated with an increase in salinity, so high Sr/Ba ratios indicate an increase in seawater depth and salinity (Chegrouche et al., 2009; Wei and Algeo, 2020). Therefore, the Sr/Ba ratio has been widely used to qualitatively evaluate paleosalinity (Zhang et al., 2017; Wei et al., 2018; Wei and Algeo, 2020). The Sr concentration and Sr/Ba ratio

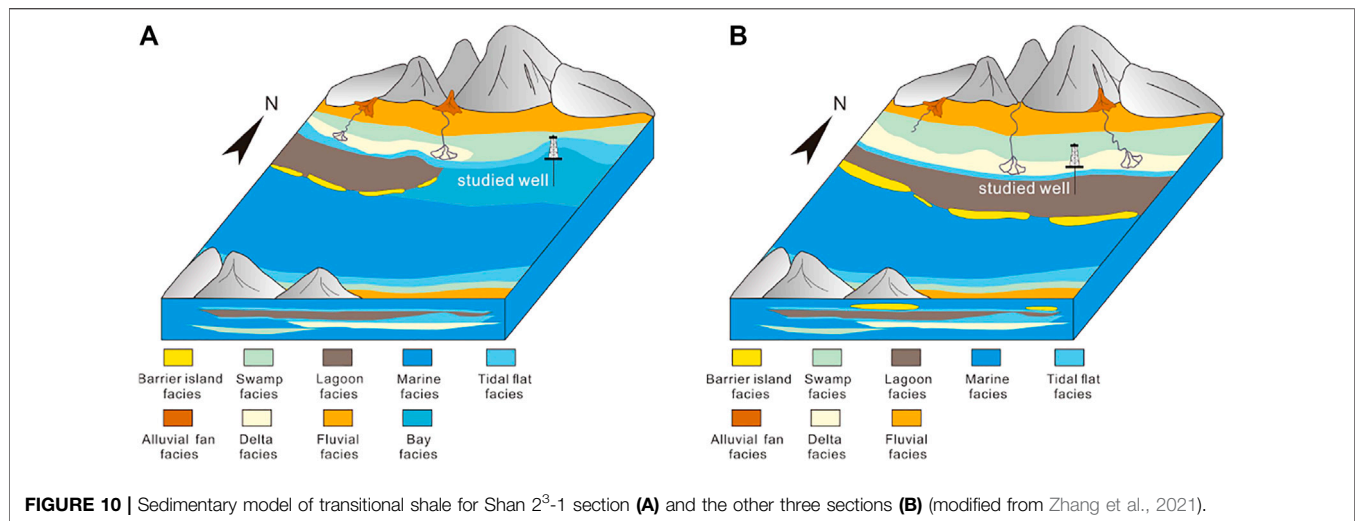


FIGURE 10 | Sedimentary model of transitional shale for Shan 2³-1 section (A) and the other three sections (B) (modified from Zhang et al., 2021).

in sedimentary rocks have a strong positive linear relationship with paleosalinity, while the Ba content is negatively correlated with paleosalinity. Because Sr and Ca are similar in atomic radius, the Sr concentration may be much higher in sediments containing carbonate components. Before evaluating paleosalinity with the Sr/Ba ratio, the influence of carbonate rocks on Sr content must be excluded.

There is no correlation between CaO and the Sr/Ba ratio in each section (Figure 8A), which can exclude the influence of carbonate components. Wei and Algeo (2020) proposed that sedimentary Sr/Ba ratios of <0.2, 0.2–0.5, and >0.5 indicate freshwater, brackish, and marine water, respectively. Sr/Ba ratios are different in different sections (Figure 8B). The Shan 2³-1 section is deposited in a brackish water–marine environment, and the average Sr/Ba ratio is 0.57. In particular, the average Sr/Ba ratio of organic-rich shale interval with high TOC is greater than 0.60, which may be greatly affected by seawater (Figure 8B). The Sr/Ba ratio of the Shan 2³-2 section is slightly lower than that of the Shan 2³-1 section, with an average of 0.52, which also reflects the sedimentary environment of brackish water. Sr/Ba ratios in the Shan 2³-3 and Shan 2³-4 sections decrease significantly, with the average values of 0.38 and 0.40, respectively, indicating a decrease in paleosalinity (Figure 8B). Combined with the change of terrestrial input index elements, it is suggested that, during the Shan 2³-3 and Shan 2³-4 period, the sea level decreased, the input of freshwater carrying terrestrial debris increased, and the influence of seawater on the sedimentary environment decreased.

Paleoredox Conditions

Trace element proxies such as U/Th, U_{EF} , and Mo_{EF} were widely used to determine the redox conditions of paleo-water. Smaller proxies reflect a higher oxidation degree, and the larger ratio reflects a stronger reduction degree (Cao et al., 2018; Liu et al., 2018; Zhang et al., 2019; He et al., 2020). High U/Th ratios were consistent with highly reducing conditions, with U/Th > 1.25 representing suboxic/anoxic environments and U/Th < 0.75 representing normal oxic sedimentary environments (Hatch and Leventhal, 1992; Jones and Manning, 1994; Tribouillard

et al., 2006). Authigenic Mo, authigenic U enrichment, and Mo–U covariant models have been used to elucidate redox conditions and water mass limitation (Algeo and Lyons, 2006; Algeo and Tribouillard, 2009; Algeo and Liu, 2020). Overall, the oxic environment showed little or no enrichment of authigenic Mo and U, while the anoxic environment showed strong enrichment of authigenic Mo and U (Algeo and Tribouillard, 2009). The U/Th values of each section are less than 0.75, suggesting that the sedimentary environment is generally inclined to oxic conditions (Figure 6). The data points of the Shan 2³ Submember are all located in the oxic area (Figure 9), which is consistent with the U/Th value. However, the variation trend of U_{EF} and Mo_{EF} shows that the authigenic Mo and U in the high TOC interval are obviously enriched (Figure 6), and it is suggested that the sedimentary environment in this interval tends to be anoxic reduction conditions.

SEDIMENTARY MODEL OF ORGANIC-RICH SHALE

During the Taiyuan period, the study area is controlled by a widespread epeiric platform. The gentle slope of the epeiric platform is easy to form a wide range of shallow water areas. Even a weak sea-level change can change the spatial distribution of sedimentary facies. During the late stage of the Taiyuan period, the central part of the study area is dominated by marine facies. The south and north of the study area are close to the provenance area, which are dominated by delta and tidal flat environments. The Shan 2³-1 section inherited the sedimentary background of the Taiyuan period. With the rapid rise of the sea level, the central part of the study area has rapidly turned to bay facies (Figure 10A), and the paleoredox condition has changed from oxic condition to anoxic. Meanwhile, the sedimentary environment is dominated by brackish water–marine seawater. The climate is relatively dry, and the influence of detrital influx is limited. These conditions benefit the enrichment of marine fauna and preservation of organic matter in organic-rich shale. From

the deposition of the Shan 2³-2 section, the sea level shows a decreasing trend, and the influence of seawater on the sedimentary environment is weakened. The frequent changes in sea levels lead to frequent changes of sedimentary facies at the location of the studied well, which are lagoon facies, tidal flat facies, and swamp facies. Shale is deposited in the lagoon environment (Figure 10B). However, as the climate gradually tends to be warm and humid at this time, the intensity of chemical weathering increases, the input of terrigenous debris increases, and the sedimentary environment is an oxic condition. The preservation of organic matter in shale cannot benefit from this condition.

CONCLUSION

- 1) Shanxi Formation Shan 2³ Submember can be divided into four sections (Shan 2³-1, Shan 2³-2, Shan 2³-3, and Shan 2³-4). High TOC interval (2.75%–10.96%, avg. 6.98%) belongs to the upper part of the Shan 2³-1 section. The high TOC interval is dominated by bay facies, which is characterized by low detrital influx proxies (Zr, 97–527 ppm, avg. 310 ppm; Ti, 1,985–7,591 ppm, avg. 3,938 ppm), relatively dry paleoclimate condition (CIA*, 41.96–92.58, avg. 75.55; Sr/Cu, 6.23–14.49, avg. 8.87), high paleosalinity proxies (Sr/Ba, 0.39–1.29, avg. 0.62), and relatively anoxic reduction condition (U_{EF}, 0.83–3.00, avg. 1.67; Mo_{EF}, 3.95–27.00, avg. 15.56).
- 2) The vertical variations of sedimentological and geochemical characteristics suggest that the other three sections are dominated by fine-grained sandstone, silty mudstone, shale, and coal, representing barrier island, tidal flat,

lagoon, and swamp facies, respectively. The paleoclimate gradually tends to be warm and humid (CIA*, 75.68–95.63, avg. 85.93; Sr/Cu, 1.19–24.18, avg. 9.92), which results in increasing the chemical weathering intensity. Meanwhile, the detrital influx proxies increase (Zr, 159–1,558 ppm, avg. 442 ppm; Ti, 840–9,309 ppm, avg. 5230 ppm), and the paleoredox condition tends to be oxic (U_{EF}, 0.51–5.23, avg. 1.07; Mo_{EF}, 0.79–18.50, avg. 3.75). The above conditions are not conducive to the preservation of organic matter in lagoon facies shale.

DATA AVAILABILITY STATEMENT

The original contributions presented in the study are included in the article/Supplementary Material, further inquiries can be directed to the corresponding author.

AUTHOR CONTRIBUTIONS

YG contributed as the major author of the article. XL conceived the project. SL, XY, and YJ collected the samples. YG, LQ, and YF analyzed the samples. All authors contributed to the article and approved the submitted version.

FUNDING

This study was funded by the Science and Technology Cooperation Project of the CNPC-SWPU Innovation Alliance (Grant no. 2020CX030101).

REFERENCES

- Algeo, T. J., and Liu, J. (2020). A Re-assessment of Elemental Proxies for Paleoredox Analysis. *Chem. Geol.* 540, 119549. doi:10.1016/j.chemgeo.2020.119549
- Algeo, T. J., and Lyons, T. W. (2006). Mo-total Organic Carbon Covariation in Modern Anoxic marine Environments: Implications for Analysis of Paleoredox and Paleohydrographic Conditions. *Paleoceanography* 21, PA1016. doi:10.1029/2004PA001112
- Algeo, T. J., and Tribouillard, N. (2009). Environmental Analysis of Paleocyanographic Systems Based on Molybdenum-Uranium Covariation. *Chem. Geol.* 268, 211–225. doi:10.1016/j.chemgeo.2009.09.001
- Bai, Y., Liu, Z., Sun, P., Liu, R., Hu, X., Zhao, H., et al. (2015). Rare Earth and Major Element Geochemistry of Eocene fine-grained Sediments in Oil Shale- and Coal-Bearing Layers of the Meihe Basin, Northeast China. *J. Asian Earth Sci.* 97 (97), 89–101. doi:10.1016/j.jseas.2014.10.008
- Berry, W. B. N. (2010). “Black Shales: An Ordovician Perspective,” in *The Ordovician Earth System* (Berkeley, California: The Geological Society of America Special), 141–147. doi:10.1130/2010.2466(09)
- Bertrand, P., Shimmield, G., Martinez, P., Grousset, F., Jorissen, F., Paterne, M., et al. (1996). The Glacial Ocean Productivity Hypothesis: the Importance of Regional Temporal and Spatial Studies. *Mar. Geol.* 130, 1–9. doi:10.1016/0025-3227(95)00166-2
- Cao, J., Yang, R., Yin, W., Hu, G., Bian, L., and Fu, X. (2018). Mechanism of Organic Matter Accumulation in Residual bay Environments: The Early Cretaceous Qiangtang Basin, Tibet. *Energy Fuels* 32, 1024–1037. doi:10.1021/acs.energyfuels.7b02248
- Caplan, M. L., and Bustin, R. M. (1998). Sedimentology and Sequence Stratigraphy of Devonian-Carboniferous Strata, Southern Alberta. *Bull. Can. Pet. Geol.* 46 (4), 487–514. doi:10.35767/gscpgbull.46.4.487
- Chegrouche, S., Mellah, A., and Barkat, M. (2009). Removal of Strontium from Aqueous Solutions by Adsorption onto Activated Carbon: Kinetic and Thermodynamic Studies. *Desalination* 235 (1-3), 306–318. doi:10.1016/j.desal.2008.01.018
- Chen D, D., Wang, J., Yan, D., Wei, H., Yu, H., and Wang, Q. (2011). Environmental Dynamics of Organic Accumulation for the Principal Paleozoic Source Rocks on Yangtze Block. *Chin. J. Geol.* 46 (1), 5–26. doi:10.3969/j.issn.0563-5020.2011.01.003
- Chen, Y., Wang, Y., Guo, M., Wu, H., Li, J., Wu, W., et al. (2020). Differential Enrichment Mechanism of Organic Matters in the marine-continental Transitional Shale in Northeastern Ordos Basin, China: Control of Sedimentary Environments. *J. Nat. Gas Sci. Eng.* 83, 103625. doi:10.1016/j.jngse.2020.103625
- Chen H, H., Li, J., Zhang, C., and Cheng, L. (2011). Discussion of Sedimentary Environment and its Geological Enlightenment of Shanxi Formation in Ordos Basin. *Acta Petrol. Sin.* 27 (8), 2213–2229.
- Dong, D., Qiu, Z., Zhang, L., Li, S., Zhang, Q., Li, X., et al. (2021). Progress on Sedimentology of Transitional Facies Shales and New Discoveries of Shale Gas. *Acta Sedimentol. Sin.* 39 (1), 28–44. doi:10.14027/j.issn.1000-0550.2021.002
- Guan, Q., Lü, X., Dong, D., and Cai, X. (2019). Origin and Significance of Organic-Matter Pores in Upper Ordovician Wufeng-Lower Silurian Longmaxi Mudstones, Sichuan Basin. *J. Pet. Sci. Eng.* 176, 554–561. doi:10.1016/j.petrol.2019.01.079
- Guan, Q., Dong, D., Zhang, H., Sun, S., Zhang, S., and Guo, W. (2021). Types of Biogenic Quartz and its Coupling Storage Mechanism in Organic-Rich Shales:

- A Case Study of the Upper Ordovician Wufeng Formation to Lower Silurian Longmaxi Formation in the Sichuan Basin, SW China. *Pet. Explor. Develop.* 48 (4), 813–823. doi:10.1016/S1876-3804(21)60068-X
- Hatch, J. R., and Leventhal, J. S. (1992). Relationship between Inferred Redox Potential of the Depositional Environment and Geochemistry of the Upper Pennsylvanian (Missourian) Stark Shale Member of the Dennis limestone, Wabaunsee County, Kansas, U.S.A. *Chem. Geol.* 99 (1/3), 65–82. doi:10.1016/0009-2541(92)90031-y
- He, Q., Dong, T., He, S., Zhai, G., Guo, X., Hou, Y., et al. (2020). Sedimentological and Geochemical Characterization of the Upper Permian Transitional Facies of the Longtan Formation, Northern Guizhou Province, Southwest China: Insights into Paleo-Environmental Conditions and Organic Matter Accumulation Mechanisms. *Mar. Pet. Geol.* 118, 104446. doi:10.1016/j.marpetgeo.2020.104446
- Hou, Y., He, S., Yang, X., Duan, W., Zhu, G., Xu, X., et al. (2015). Geochemical Characteristics and Development Model of Transitional Source Rocks during the continental Margin Rifting Stage, Bonaparte Basin, Australia. *Pet. Geol. Exp.* 37 (3), 374–382. doi:10.11781/sydz201503374
- Huang, B., Yan, Y., Piper, J. D. A., Zhang, D., Yi, Z., Yu, S., et al. (2018). Paleomagnetic Constraints on the Paleogeography of the East Asian Blocks during Late Paleozoic and Early Mesozoic Times. *Earth Sci. Rev.* 186, 8–36. doi:10.1016/j.earscirev.2018.02.004
- Jones, B., and Manning, D. A. C. (1994). Comparison of Geochemical Indices Used for the Interpretation of Palaeoredox Conditions in Ancient Mudstones. *Chem. Geol.* 111 (111), 111–129. doi:10.1016/0009-2541(94)90085-X
- Kuang, L., Dong, D., He, W., Wen, S., Sun, S., Li, S., et al. (2020). Geological Characteristics and Development Potential of Transitional Shale Gas in the East Margin of the Ordos Basin, NW China. *Pet. Explor. Develop.* 47 (3), 435–446. doi:10.11698/PED.2020.03.0110.1016/s1876-3804(20)60066-0
- Li, Y., Zhang, T., Ellis, G. S., and Shao, D. (2017). Depositional Environment and Organic Matter Accumulation of Upper Ordovician-Lower Silurian marine Shale in the Upper Yangtze Platform, South China. *Palaeogeogr. Palaeoclimatol. Palaeoecol.* 466, 252–264. doi:10.1016/j.palaeo.2016.11.037
- Li, Y., Yang, J., Pan, Z., Meng, S., Wang, K., and Niu, X. (2019). Unconventional Natural Gas Accumulations in Stacked Deposits: A Discussion of Upper Paleozoic Coal-Bearing Strata in the East Margin of the Ordos Basin, China. *Acta Geol. Sin. English Edition* 93 (1), 111–129. doi:10.1111/1755-6724.1363810.1111/1755-6724.13767
- Liang, Q., Zhang, X., Tian, J., Sun, X., and Chang, H. (2018). Geological and Geochemical Characteristics of marine-continental Transitional Shale from the Lower Permian Taiyuan Formation, Taikang Uplift, Southern North China Basin. *Mar. Pet. Geol.* 98, 229–242. doi:10.1016/j.marpetgeo.2018.08.027
- Liu, Z., Algeo, T. J., Guo, X., Fan, J., Du, X., and Lu, Y. (2017). Paleo-environmental Cyclicity in the Early Silurian Yangtze Sea (South China): Tectonic or Glacio-Eustatic Control? *Palaeogeogr. Palaeoclimatol. Palaeoecol.* 466, 59–76. doi:10.1016/j.palaeo.2016.11.007
- Liu, S., Wu, C., Li, T., and Wang, H. (2018). Multiple Geochemical Proxies Controlling the Organic Matter Accumulation of the marine-continental Transitional Shale: A Case Study of the Upper Permian Longtan Formation, Western Guizhou, China. *J. Nat. Gas Sci. Eng.* 56, 152–165. doi:10.1016/j.jngse.2018.06.007
- Liu, Q., Li, P., Jin, Z., Liang, X., Zhu, D., Wu, X., et al. (2021). Preservation of Organic Matter in Shale Linked to Bacterial Sulfate Reduction (BSR) and Volcanic Activity under marine and Lacustrine Depositional Environments. *Mar. Pet. Geol.* 127, 104950. doi:10.1016/j.marpetgeo.2021.104950
- Luo, W., Hou, M., Liu, X., Huang, S., Chao, H., Zhang, R., et al. (2018). Geological and Geochemical Characteristics of marine-continental Transitional Shale from the Upper Permian Longtan Formation, Northwestern Guizhou, China. *Mar. Pet. Geol.* 89, 58–67. doi:10.1016/j.marpetgeo.2017.06.029
- McLennan, S. M. (2001). Relationships between the Trace Element Composition of Sedimentary Rocks and Upper continental Crust. *Geochem. Geophys. Geosyst.* 2, 2000gc000109. doi:10.1029/2000gc000109
- Murphy, A. E., Sageman, B. B., Hollander, D. J., Lyons, T. W., and Brett, C. E. (2000). Black Shale Deposition and Faunal Overturn in the Devonian Appalachian Basin: Clastic Starvation, Seasonal Water-Column Mixing, and Efficient Biolimiting Nutrient Recycling. *Paleoceanography* 15, 280–291. doi:10.1029/1999PA000445
- Nesbitt, H. W., and Young, G. M. (1982). Early Proterozoic Climates and Plate Motions Inferred from Major Element Chemistry of Lutites. *Nature* 299 (5885), 715–717. doi:10.1038/299715a0
- Price, J. R., and Velbel, M. A. (2003). Chemical Weathering Indices Applied to Weathering Profiles Developed on Heterogeneous Felsic Metamorphic Parent Rocks. *Chem. Geol.* 202, 397–416. doi:10.1016/j.chemgeo.2002.11.001
- Qiu, Z., and Zou, C. (2020). Controlling Factors on the Formation and Distribution of "Sweet-Spot Areas" of marine Gas Shales in South China and a Preliminary Discussion on Unconventional Petroleum Sedimentology. *J. Asian Earth Sci.* 194, 103989. doi:10.1016/j.jseas.2019.103989
- Qiu, Z., Shi, Z. S., Dong, D. Z., Lu, B., Zhang, C., Zhou, J., et al. (2016). Geological Characteristics of Source Rock and Reservoir of Tight Oil and its Accumulation Mechanism: a Case Study of Permian Lucaogou Formation in Jimusar Sag, Junggar Basin. *Pet. Explor. Develop.* 43, 928–939. doi:10.1016/S1876-3804(16)30118-5
- Rachold, V., and Brumsack, H. J. (2001). Inorganic Geochemistry of Albian Sediments from the Lower Saxony basin, NW German: Paleoenvironmental Constraints and Orbital Cycles. *Palaeogeogr. Palaeoclimatol. Palaeoecol.* 174, 123–144. doi:10.1016/S0031-0182(01)00290-5
- Sarki Yandoka, B. M., Abdullah, W. H., Abubakar, M. B., Hakimi, M. H., and Adegoke, A. K. (2015). Geochemical Characterisation of Early Cretaceous Lacustrine Sediments of Bima Formation, Yola Sub-basin, Northern Benue Trough, NE Nigeria: Organic Matter Input, Preservation, Paleoenvironment and Palaeoclimatic Conditions. *Mar. Pet. Geol.* 61, 82–94. doi:10.1016/j.marpetgeo.2014.12.010
- Sun, Z., Wang, Y., Wei, Z., Zhang, M., Wang, G., and Wang, Z. (2017). Characteristics and Origin of Desorption Gas of the Permian Shanxi Formation Shale in the Ordos Basin, China. *Energy Explor. Exploit.* 35 (6), 792–806. doi:10.1177/0144598717723564
- Tang, Q., Zhou, L., Chen, L., Tan, X., and Wang, G. (2021). Development Characteristics of Shale Lithofacies in the Longmaxi Formation and Their Main Controlling Factors in the Changning Area, South Sichuan Basin, SW China. *Front. Earth Sci.* 9, 775657. doi:10.3389/feart.2021.775657
- Tribouillard, N., Algeo, T. J., Lyons, T., and Riboulleau, A. (2006). Trace Metals as Paleoredox and Paleoproductivity Proxies: An Update. *Chem. Geol.* 232 (1/2), 12–32. doi:10.1016/j.chemgeo.2006.02.012
- Tribouillard, N., Algeo, T. J., Baudin, F., and Riboulleau, A. (2012). Analysis of marine Environmental Conditions Based Onmolybdenum-Uranium Covariation-Applications to Mesozoic Paleooceanography. *Chem. Geol.* 324–325, 46–58. doi:10.1016/j.chemgeo.2011.09.009
- Wang, Y., Guo, W., and Zhang, G. (1979). Application of Some Geochemical Indicators in Determining of Sedimentary Environment of the Funing Group (Paleogene), Jin-Hu Depression, Kiangsu Province. *J. Tongji Univ.* 2, 51–60.
- Wang, A. (1996). Discriminant Effect of Sedimentary Environment by the Sr/Ba Ratio of Different Existing Forms. *Acta Sedimentol. Sin.* 3 (2), 297–304. doi:10.1002/jts.2490030210
- Wedepohl, K. H. (1995). The Composition of the continental Crust. *Geochim. Cosmochim. Acta* 59 (7), 1217–1232. doi:10.1016/0016-7037(95)00038-2
- Wei, W., and Algeo, T. J. (2020). Elemental Proxies for Paleosalinity Analysis of Ancient Shales and Mudrocks. *Geochim. Cosmochim. Acta* 287, 341–366. doi:10.1016/j.gca.2019.06.034
- Wei, W., Algeo, T. J., Lu, Y., Lu, Y., Liu, H., Zhang, S., et al. (2018). Identifying marine Incursions into the Paleogene Bohai Bay Basin lake System in Northeastern China. *Int. J. Coal Geol.* 200, 1–17. doi:10.1016/j.coal.2018.10.001
- Wei, Z., Wang, G., Wang, Y., Ma, X., Zhang, T., He, W., et al. (2020). Geochemical and Geological Characterization of Marine-Continental Transitional Shale: A Case Study in the Ordos Basin, NW China. *Acta Geol. Sin. English Edition* 94 (3), 809–821. doi:10.1111/1755-6724.13888
- Wei, C., Dong, T., He, Z., He, S., He, Q., Yang, R., et al. (2021). Major, Trace-Elemental and Sedimentological Characterization of the Upper Ordovician Wufeng-Lower Silurian Longmaxi Formations, Sichuan Basin, south China: Insights into the Effect of Relative Sea-Level Fluctuations on Organic Matter Accumulation in Shales. *Mar. Pet. Geol.* 126, 104905. doi:10.1016/j.marpetgeo.2021.104905
- Wolgemuth, K., and Broecker, W. S. (1970). Barium in Sea Water. *Earth Planet. Sci. Lett.* 8 (5), 372–378. doi:10.1016/0012-821X(70)90110-X
- Wu, J., Wang, H., Shi, Z., Wang, Q., Zhao, Q., Dong, D., et al. (2021). Favorable Lithofacies Types and Genesis of marine-continental Transitional Black Shale:

- A Case Study of Permian Shanxi Formation in the Eastern Margin of Ordos Basin, NW China. *Pet. Explor. Develop.* 48 (6), 1315–1328. doi:10.1016/S1876-3804(21)60289-6
- Xie, G., Shen, Y., Liu, S., and Hao, W. (2018). Trace and Rare Earth Element (REE) Characteristics of Mudstones from Eocene Pinghu Formation and Oligocene Huangang Formation in Xihu Sag, East China Sea Basin: Implications for Provenance, Depositional Conditions and Paleoclimate. *Mar. Pet. Geol.* 92, 20–36. doi:10.1016/j.marpetgeo.2018.02.019
- Xu, Q., Liu, B., Ma, Y., Song, X., Wang, Y., and Chen, Z. (2017). Geological and Geochemical Characterization of Lacustrine Shale: A Case Study of the Jurassic Da'anzhai Member Shale in the central Sichuan Basin, Southwest China. *J. Nat. Gas Sci. Eng.* 47, 124–139. doi:10.1016/j.jngse.2017.09.008
- Yang, C., Zhang, J., Tang, X., Ding, J., Zhao, Q., Dang, W., et al. (2017). Comparative Study on Micro-pore Structure of marine, Terrestrial, and Transitional Shales in Key Areas, China. *Int. J. Coal Geol.* 171, 76–92. doi:10.1016/j.coal.2016.12.001
- Zhang, S., Zhang, B., Bian, L., Jin, Z., Wang, D., Zhang, X., et al. (2005). Development Constraints of marine Source Rocks in China. *Earth Sci. Front.* 12 (3), 39–48.
- Zhang, X., Lin, C., Zahid, M. A., Jia, X., and Zhang, T. (2017). Paleosalinity and Water Body Type of Eocene Pinghu Formation, Xihu Depression, East China Sea Basin. *J. Pet. Sci. Eng.* 158, 469–478. doi:10.1016/j.petro.2017.08.074
- Zhang, J., Li, X., Zhang, X., Zhang, M., Cong, G., Zhang, G., et al. (2018). Geochemical and Geological Characterization of marine-continental Transitional Shales from Longtan Formation in Yangtze Area, South China. *Mar. Pet. Geol.* 96, 1–15. doi:10.1016/j.marpetgeo.2018.05.020
- Zhang, K., Song, Y., Jiang, S., Jiang, Z., Jia, C., Huang, Y., et al. (2019). Mechanism Analysis of Organic Matter Enrichment in Different Sedimentary Backgrounds: A Case Study of the Lower Cambrian and the Upper Ordovician-Lower Silurian, in Yangtze Region. *Mar. Pet. Geol.* 99, 488–497. doi:10.1016/j.marpetgeo.2018.10.044
- Zhang, K., Liu, R., Liu, Z., Li, L., Wu, X., and Zhao, K. (2020). Influence of palaeoclimate and hydrothermal activity on organic matter accumulation in lacustrine black shales from the Lower Cretaceous Bayingebi Formation of the Yin'e Basin, China. *Palaeogeogr. Palaeoclimatol. Palaeoecol.* 560, 110007. doi:10.1016/j.palaeo.2020.110007
- Zhang, L., Dong, D., Qiu, Z., Wu, C., Zhang, Q., Wang, Y., et al. (2021). Sedimentology and Geochemistry of Carboniferous-Permian marine-continental Transitional Shales in the Eastern Ordos Basin, North China. *Palaeogeogr. Palaeoclimatol. Palaeoecol.* 571 (1-3), 110389. doi:10.1016/j.palaeo.2021.110389
- Zou, C., Dong, D., Wang, Y., Li, X., Huang, J., Wang, S., et al. (2015). Shale Gas in China: Characteristics, Challenges and Prospects (I). *Pet. Explor. Develop.* 42 (6), 753–767. doi:10.1016/S1876-3804(15)30072-0
- Zou, C., Zhu, R., Chen, Z.-Q., Ogg, J. G., Wu, S., Dong, D., et al. (2019). Organic-matter-rich Shales of China. *Earth Sci. Rev.* 189, 51–78. doi:10.1016/j.earscirev.2018.12.002

Conflict of Interest: XL and SL were employed by the PetroChina Coalbed Methane Company. IQ was employed by the CNPC Chuanqing Drilling Engineering Co., Ltd.

The remaining authors declare that the research was conducted in the absence of any commercial or financial relationships that could be construed as a potential conflict of interest.

Publisher's Note: All claims expressed in this article are solely those of the authors and do not necessarily represent those of their affiliated organizations or those of the publisher, the editors, and the reviewers. Any product that may be evaluated in this article, or claim that may be made by its manufacturer, is not guaranteed or endorsed by the publisher.

Copyright © 2022 Gu, Li, Qi, Li, Jiang, Fu and Yang. This is an open-access article distributed under the terms of the Creative Commons Attribution License (CC BY). The use, distribution or reproduction in other forums is permitted, provided the original author(s) and the copyright owner(s) are credited and that the original publication in this journal is cited, in accordance with accepted academic practice. No use, distribution or reproduction is permitted which does not comply with these terms.